Electrical and Thermal Performance Evaluation of a District Heating System Composed of Asymmetric low concentration PVT Solar Collector Prototypes

Diogo Cabral[1], João Costeira[2], João Gomes[1]

[1] Department of Building, Energy and Environmental Engineering, University of Gävle, Sweden

[2] Department of Earth Sciences, University of Minho, Portugal

Abstract

Photovoltaic-Thermal (PVT) solar collectors generate electricity and heat from the same gross area. The annual electrical and thermal yields of these systems are dependent on the PVT collector technology, as well as the climate and the type of solar thermal system implemented. This review presents an evaluation of a district heating system composed of 20 asymmetric hybrid low concentrator PVT (C-PVT) solar collector prototypes. The system is installed in a South wall facade in order to maximise the available space (with a tilt of 20º and an orientation of 5ºW). The thermal system is connected to the district heating network, thus heating the University buildings. On the other hand, the electrical system is grid-connected, where it feeds the grid directly. Real measurement data has been collected and compared with a thermal (through ScenoCalc tool) and electrical performance models. The annual thermal and electrical yield achieved 86% and 89% of the simulated thermal and electrical yield, respectively.

Keywords: C-PVT, System analysis, Electrical and Thermal evaluation

1. Introduction

1.1. State of Art

Concentrator Photovoltaic-Thermal (C-PVT) solar collectors can be based on Compound Parabolic Collector (CPC) or on parabolic trough collector (Sharaf and Orhan, 2015). C-PVT collectors are hybrid solar collectors that simultaneously generate electrical (through PV cells) and thermal energy (through the solar radiation absorbed by the PV cells that is not converted into electricity).

Concentrating solar collectors re-direct the solar radiation (both beam and diffuse radiation) that passes through an aperture into the receiver over ranges of incidence angles within wide limits (thus defining the acceptance half-angle, θ_c). For systems of low concentration ratio, part of the diffuse radiation will be reflected into the receiver, with this amount being dependent on the acceptance angle of the concentrator (Duffie and Beckman, 2013).

According to Zondag (2018), this solar collector technology can be classified according to their design (unglazed, glazed, and concentrating), PV cell technology, and their heat transfer medium (water and air). C-PVT collectors can also be classified according to their concentration ratio, such as low, medium or high concentration, having the possibility of both stationary and tracked operation (Stine and Harrigan, 1986).

It is acknowledged that each collector technology matches specific temperature stages and corresponding suitable applications, especially if the concentrating technology is applied since higher concentration leads to higher temperatures. Previous studies showed that the efficiency of PV cells is temperature dependent and that for every degree increase in temperature, the cell efficiency decreases around 0.4%, and for that reason, it is necessary to remove and harvest the excess heat by means of an active cooling system.

In order to carry out the excess thermal energy generated by the PV cells, an active cooling fluid is used (generally water with a percentage of glycol to prevent the fluid to freeze), which leads to a decrease in temperature on the solar cells, increasing their overall efficiency. This way, the waste heat harvested by the cooling fluid can be used as a cogenerated product and for heating applications (Kramer and Helmers, 2013).

1.2. Maximum Reflector Concentration geometry concept

Several studies on asymmetric concentrating collectors have been reported by Rabl (1976), Mills and Giutronich (1978), Welford and Winston (1989), Tripanagnostopoulos et al. (1999, 2000), Adsten et al. (2005) and Bernardo et al. (2013). These studies led to a novel truncated geometry called Maximum Reflector

Selection and/or peer review under responsibility of Scientific Committee
doi:10.18086/eurosun2018.02.15 Available at http://proceedings.ises.org

Concentration (MaReCo) collector, due to the asymmetric solar radiation over the year at high latitudes, more specifically in Sweden (Adsten et al., 2005).
The MaReCo suits high latitudes due to the low solar altitude and the large cloud coverage during winter time. The generally form of the MaReCo reflector trough (Fig. 1) consists of two parabolic reflectors with their individual optical axis tilted 20° and 65° from the bottom side of the receiver (point 1), collecting all the upcoming irradiation between a solar altitude of 20° and 65° i.e. the tilt of the back and front reflector (Fig. 1) (Nilsson, 2005).
The front reflector (section A) reflects most of the irradiation during summer months, having the highest annual output, between both reflectors. The back reflector (sections B and C) reflects more during the rest of the year. The optical axis from the parabola defines the lower and upper acceptance angles. As shown in Fig. 1 the reflector is divided into three sections A, B and C. Section A consists in a lower side parabola extended between points 1 and 4, with the optical axis along the upper acceptance angle and its focal point on the upper part of the receiver (point 5). The circular section between points 1 and 2 characterizes section B, the section that reflects the light rays into the backside of the reflector.
This section has the particularity to replace a hypothetical absorber between point 2 and the focus (dotted line between point 2 and 5) with the back side of the absorber described as the line that connects the point 1 and 5. The lower tip of the absorber can be placed anywhere in section B. The last section, corresponding to the section C is the upper parabolic reflector with the optical axis along the lower acceptance angle and its focus at point 5, represented between points 2 and 3.

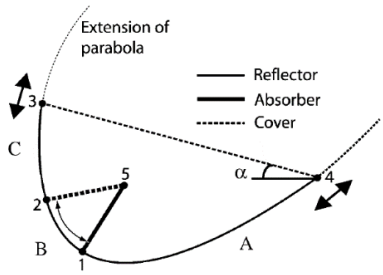

Fig. 1. Sketch of the basic MaReCo design. Part A is the lower parabolic reflector extended from point 1–4; Part B is the connecting circular reflector extended from point 1–2; Part C is the upper parabolic reflector extended from the point 2–3. The cover glass is found between points 3 and 4. The position of the cover glass varies along the extended parabola depending on the truncation is the aperture tilt (Adsten et al., 2005).

The position of the cover glass (dotted line between points 3 and 4) can vary along the extensions of the parabola depending on the desired truncation. This position can be obtained by varying the position of the reflector sheet along the extended parabolas, where the maximum annual irradiation is obtained.
The current reflector geometry has a bifacial PVT (with coolant filled tubes) receiver that is parallel to the cover glass, and two sections B and C, as the ones presented in Fig. 1. The collector geometry is described more methodically by Bernardo et al. (2013) and can be seen in the following Fig. 2.

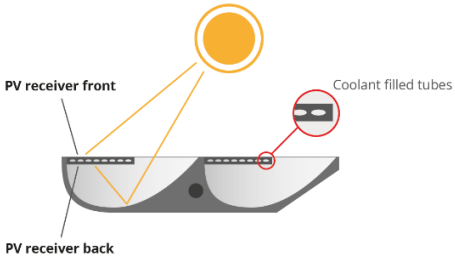

Fig. 2. Profile view of the MaReCo prototype concept, composed of two troughs and two PVT receivers with eight elliptical channels each.

1.3. Impact of shading in C-PVT solar collectors

Stationary solar C-PVT collectors use reflectors, which normally cause non-uniform distribution of light on the PV cell string. This non-uniform distribution may also be a consequence of partial shading that can arise from many different effects (clouds, reflector length limitations, shadows and dust or any sort of dirtiness), which in the solar PV modules, may lead to hot spots and cause permanent damage to the cells, as well as lowering the current of the whole string. Partial shading has a stronger impact on the electrical efficiency than

on the thermal efficiency of PV/PVT systems, since non-uniform radiation in one cell increases the series resistance losses. This effect may induce the developments of hotspots in the solar PV module (Woyte et al., 2003), which may cause permanent damage to the cells that are shaded. The effect is reinforced in a string of series connected cells or arrays and it is always present in compound parabolic concentrators (CPC), as Rabl (1976) presented. In mismatching operating conditions (due to manufacturing tolerances, ageing, different orientation of the solar panels), the energetic efficiency of the PV/PVT systems is strongly compromised.
A C-PVT (non-tracking), to be able to work at its full potential (electrically), needs to ensure that the reflected image of the receiver in the reflector stays as much as possible in the reflector boundaries. At lower solar altitudes (sunrise and sunset) the reflected image in the reflector is not complete, leading to a lower output (as the reflected image is partially out of the reflector boundaries). A way to avoid this effect is to use bypass diodes that allow the current to flow in a different path, shutting down only partially the string (Gomes et al., 2014).

Nomenclature

Symbol	Description [Unit]
θ_c	Acceptance half-angle [°]
t_a	Ambient temperature [°C]
G_b	Beam irradiance [W/m^2]
C_i	Concentration factor [–]
b_0	Constant for incident angle modifier
G_d	Diffuse irradiance [W/m^2]
c_5	Effective thermal capacity [J/m^2.K]
$\eta_{el,STC}$	Electrical efficiency at standard testing conditions [–]
c_1	Heat loss coefficient at (t_m - t_a) = 0 [W/m^2.K]
θ	Incidence angle [°]
$K_{\theta b}(\theta_L,\theta_T)$	Incidence angle modifier for beam radiation [–]
$K_{\theta d}$	Incidence angle modifier for diffuse radiation[–]
E_l	Long wave irradiance (λ > 3μm) [W/m^2]
t_m	Mean fluid temperature [°C]
$\eta_{0,b}$	Peak collector efficiency at ΔT = 0 K [–]
c_8	Radiation losses [W/m^2.K^4]
ρ	Reflectivity [%]
c_4	Sky temperature dependence of heat loss coefficient [–]
P_{el}	Specific electrical power output [W/m^2]
Q_{th}	Specific thermal power output [W/m^2]
u	Surrounding air speed [m/s]
β	Temperature coefficient of electrical power [%/K]
c_2	Temperature dependence of heat loss coefficient [W/m^2.K^2]
c_6	Wind dependence of the zero loss efficiency [s/m]
c_3	Wind speed dependence of heat loss coefficient [J/m^3.K]

Subscripts

CPC	Compound Parabolic Concentrators
C-PVT	Concentrating Photovoltaic-Thermal
IAM	Incidence Angle Modifier
MaReCo	Maximum Reflector Concentration
PVT	Photovoltaic-Thermal
ScenoCalc	Solar Collector Energy Output Calculator
T	Thermal

2. Methodology

2.1. Prototype concept description

The asymmetric C-PVT solar collector prototype has a solar glazing protection, being supported by a plastic and metal structure. This glass cover is made of low iron glass with a solar transmittance of 95% according to the international standard ISO 9050 for solar thermal technologies. The end gables are composed of acrylic materials with a transmittance of around 90%. Solar cells are laminated with a highly transparent and electrically insulated silicone (transparency of 96% for PV and 93% for solar thermal) on both sides of the thermal absorber, where a heat transfer medium runs through the channels in order to extract the excess heat released by the PV cells. The upper receiver side works as a standard PV module since it does not have concentration, while the lower receiver (receiver side that faces the reflector) side receives the concentrated reflected sunlight by the reflector. The prototype concept has an overall concentration factor of 1.5. The

reflector material is made of anodized aluminium with a total solar reflectance of 95% for solar thermal (measured according to norm ASTM891-87) and a total light reflectance of 98% for PV. The electrical part of the collector consists of eight cell strings connected in parallel, four on the top side and four on the bottom side. It is composed by two troughs, thus each of them has four cell strings, two at the top side and two at the bottom side. Each receiver side has 2 cell strings, with a layout of 19-19 cells (corresponding to a 1/6 full size monocrystalline solar cell) connected in series, thus a total of 152 cells per trough and 304 cells per collector. The prototype concept has an optical and electrical efficiency of 44% and 8%, respectively, and a temperature dependence of 0.43%/ºC. The collector description has been further discussed by Bernardo et al. (2013) and Fig. 3 presents a profile view of the prototype and how the reflector works (i.e. the focal line stays within the receiver boundaries until the sun passes the 0° in transversal direction).

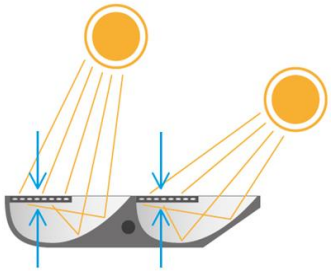

Fig. 3. Profile view of the MaReCo prototype concept, composed of two troughs.

A PVT system configuration and their annual yields were discussed in various publications have been described. Therefore, this paper aims at providing a consistent comparison of the electrical and thermal yield from an electrical and thermal performance model with real data collection, for 20 asymmetric C-PVT prototypes (with hand soldering cell strings) connected to the district heating network. The reflector geometry was developed for thermal collectors for high latitudes, at low working inlet and outlet temperatures (Adsten et al., 2005). Both the simulation and real data collection are for the same installation which is located in Gävle, at the University of Gävle (Sweden). This comparative assessment approach allows an efficient comparison between real data and simulated data for PVT collector technologies (in this study case, an asymmetric geometry), type of solar PVT system, and location.

The focus of the assessment is explicitly placed on the specific electrical and thermal yields of the collector within the context of the given system with its dynamic interaction of collector, system, and weather. The electrical and thermal yields are discussed, where the system yield is evaluated, and general conclusions on the energetic performance of the low concentration PVT collector prototype technology were drawn.

The evaluation of the thermal yield is made by means of a stationary mean working fluid temperature simulation tool called Solar Collector Energy Output Calculator (ScenoCalc), based on a thermal performance model used for test methods for solar thermal collectors described in ISO 9806:2013. The estimation of the electrical yield is based on an electrical performance model presented by Lämmle et al. (2017).

2.2. System description

The annual average distribution temperatures in District Heating grids has been 86ºC for the supply pipes and 47ºC for the return pipes (Werner, 2017). The systems' inlet and outlet temperature have been selected by the average inlet and outlet temperature values registered for the given year, where the working temperatures varied between 43ºC and 62ºC. Note that the temperature values were taken for the whole year, thus having an error associated when comparing them to the instant values registered every hour at the system. Low concentrating PVT collectors perform significantly better at low working inlet and outlet temperatures, thus selecting high working temperatures will lead the system to underperform significantly. For that, several sensors have been installed in the system in order to monitor the data throughout the year.

The system is placed at the wall facade of a laboratory building at Gävle University (Sweden), is divided into three rows with 8, 4 and 8 collector prototypes, as can be seen in Fig. 4.

Fig. 4. Wall facade installation of asymmetric C-PVT solar collector prototypes at Gävle University, Sweden.

The thermal system (Fig. 5) is composed of five simple parallel loops with four collectors per loop, where each loop has one sensor installed (Fig. 5, from sensor 1 to 5). The system is connected to a heat exchanger, which is connected to the district heating network, providing heat to the University buildings.
The following Fig. 5 shows the layout of the thermal system with the respective components.

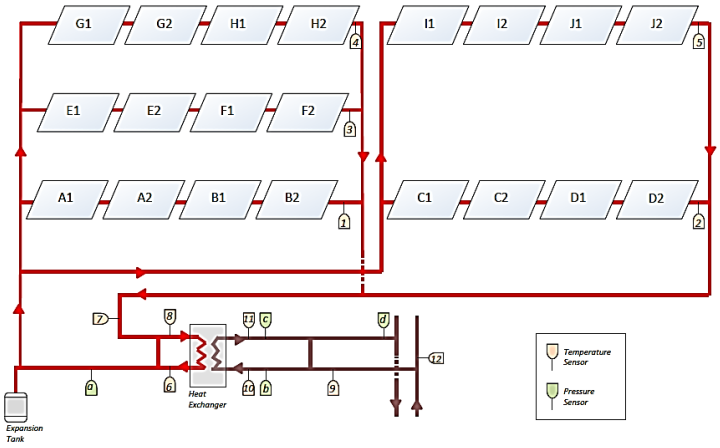

Fig. 5. System thermal layout, connected to the district heating network.

On the other hand, the electrical system presented in Fig. 6, is composed of two systems connected directly to the grid. System 1 is composed by four groups of two collectors (for a total peak power of 1.8 kW_p) and system 2 by six groups of two units (for a total peak power of 3 kW_p). Each system has an inverter and per two collectors a power optimizer is used. The electrical layout of the system can be seen in the following Fig. 6.

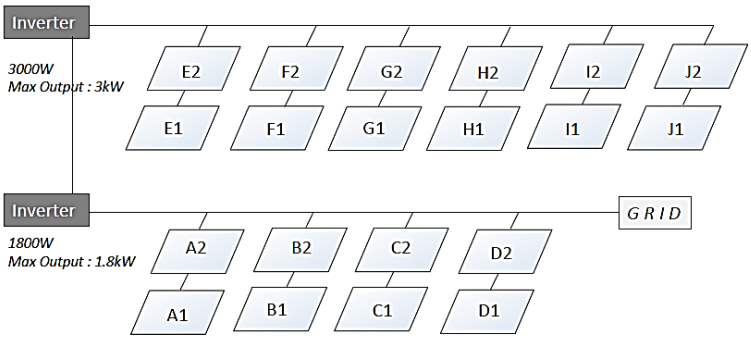

Fig. 6. Electrical system layout, divided into two systems. System 1 with 1.8 kW_p and system 2 with 3 kW_p.

2.3. Performance models

In order to accurately calculate both thermal and electrical yield of the different geometries, the collector parameters have been taken into account and normalized to the gross area of the C-PVT, according to the international standard for solar thermal collectors ISO 9806:2013. The thermal and electrical parameters were obtained at the Solar Energy Laboratory (LES), in Lisbon. The testing is based on test methods for solar thermal

collectors described in ISO 9806:2013.

2.3.1. *Thermal performance model*

The thermal collector parameters for the system, such as the IAM factor for diffused radiation ($K_{\theta d}$, that it is given by the inverse of the concentration factor), heat loss coefficient (c_1 = 3.5 W/m^2.K), temperature dependent heat loss coefficient (c_2 = 0.013 W/m^2.K^2), and the collector optical efficiency for beam radiation ($\eta_{0,b}$ = 0.44) have been employed into Eq. (1).
The prototype concept is characterized by an asymmetric transversal IAM due to the asymmetric MaReCo geometry presented by Adsten et al. (2005), and it is presented below in Fig. 7.

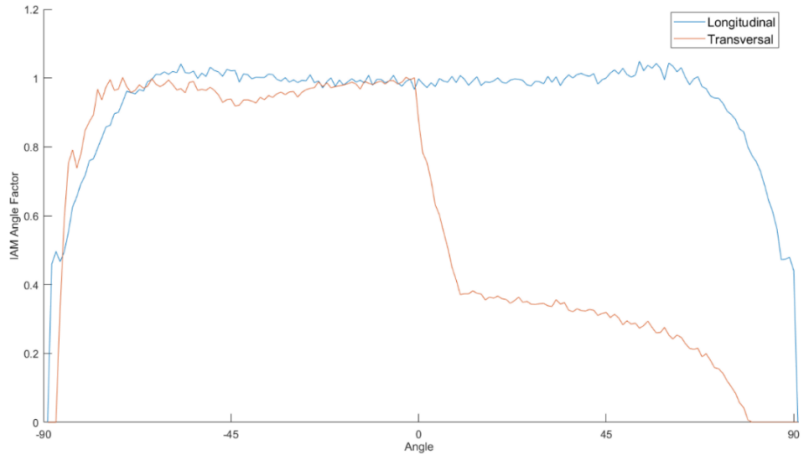

Fig. 7. Transversal (asymmetric red line) and longitudinal (symmetric blue line) IAM for the asymmetric prototype with a MaReCo geometry.

Both transversal and longitudinal IAMs have been normalized for normal incidence as suggested in ISO 9806:2013 for heating solar collectors.
Due to its geometry, the receivers behave differently from each other. The top receiver (receiver facing the sky) acts as a standard PV module, having a symmetrical transversal maximum efficiency curve. On the other hand, the bottom receiver (receiver facing the reflector) is highly dependent on the suns' position. When the sun goes over the 0° transversal, the MaReCo geometry has no ability to redirect the sun rays towards the receiver, thus the steep decrease seen in Fig. 7.
A simplified quasi-dynamic model for thermal collector performance model has been employed, taking into account the dependence on direct and diffuse radiation, mean fluid temperature and incidence angle modifiers. Eq. (1) shows the energy balance equation of a thermal collector, described in ISO 9806:2013 and used in ScenoCalc.

$$Q_{th} = \eta_{0,b} \cdot (K_{\theta b}(\theta_L,\theta_T) \cdot G_b + K_{\theta d} \cdot G_d) - c_1 \cdot (t_m - t_a) - c_2 \cdot (t_m - t_a)^2 - c_3 \cdot u \cdot (t_m - t_a) + c_4 \cdot (E_L - \sigma \cdot t_a^4) - c_5 \cdot \frac{dt_m}{dt} \quad (1)$$

Where $\eta_{0,b}$ stands for optical efficiency, $K_{\theta b}(\theta_L,\theta_T)$ and $K_{\theta d}$ for the IAM coefficients factors for direct and diffuse solar radiation, respectively. The heat losses are given by the coefficients c_1 and c_2 in respect to the difference between mean fluid temperature t_m and the ambient temperature t_a. The coefficient c_5 is the effective thermal capacity, which describes the dependency to the derivate in time of the mean fluid temperature $\frac{dt_m}{dt}$. This parameter has been removed due to the fact that the temperature is static with a system of no thermal mass. Both coefficients c_3 and c_4 for the given glazed collector prototype are close to zero, due to neglectable wind speed dependence. Eq. (2) shows the final equation used to estimate the thermal yield.

$$Q_{th} = \eta_{0,b} \cdot (K_{\theta b}(\theta_L,\theta_T) \cdot G_b + K_{\theta d} \cdot G_d) - c_1 \cdot (t_m - t_a) - c_2 \cdot (t_m - t_a)^2 \quad (2)$$

2.3.2. *Electrical performance model*

A simplified electrical performance model was based in the a PVT electrical performance model suggested by Lämmle et al. (2017), which takes into account different parameters, such as direction of beam and diffuse radiation, the instantaneous performance ratio (PR) due to incidence angle losses ($PR_{IAM} = = 1 - b_0 \cdot (\frac{1}{\cos\theta} - 1)$; Duffie and Beckman, 2013), the temperature dependence of the electrical efficiency ($PR_T = 1 - \beta \cdot (t_{cell,PVT} - t_a)$; Skoplaki and Palyvos, 2009), and standard panel efficiency $\eta_{el,STC}$. The cell temperature in PVT collectors $t_{cell,PVT}$ presented by Lämmle et al. (2016) was simplified as the fluid mean temperature t_m due to lack of sensors in this particular area. Due to the concentration factor of the PVT in the analysis, the low irradiance behaviour PR_G presented by Heydenreich et al. (2008) was not considered, thus the instantaneous specific electrical power output P_{el} is given by the following Eq. (3).

$$P_{el} = \eta_{el,STC} \cdot PR_{IAM} \cdot PR_T \cdot G \quad (3)$$

Where the temperature coefficient of electrical power β and the standard panel electrical efficiency $\eta_{el,STC}$ are 0.43 %/K and 8 %, respectively.

3. Results

In the following section, the electrical and thermal energy yield assessment are presented and discussed. The estimation of the electrical and thermal yields have been determined by using meteorological data records measured at the installation site, with hourly time steps. The system is located in Gävle, Sweden (Lat. 60.67°N; Long. 17.17°E) and the year is characterised by an average global irradiation in the horizontal plane of 996 kWh/m^2/year. It is important to state that the collectors in the analysis are prototypes with handmade cell string soldering, leading to some default collectors, and thus lowering the overall performance of the system.

3.1. *System analysis*

In order to perform the simulations a comparison with the irradiation data, the Copernicus Atmosphere Monitoring Service (CAMS) radiation service has been made. This service provides measurements based on satellite data with a time step from 1 min to 1 month. The Global, Direct and Diffuse Radiation can be queried for both the actual weather conditions and for clear sky conditions. On a cloudless day, this data is very accurate, but the exact time resolution on a partially cloudy day is somewhat lost due to the geographic resolution of the satellite data being coarse. Still, it results in a very accurate value on average, with a variation of around 2%.

This review focus on an asymmetric low concentrator PVT solar collector technology, thus the electrical system losses regarding soiling and shading (up to 5%) presented by Dobos (2014) are not implemented. Dobos (2014) also quantified the different electrical system losses (up to 16%) for systems composed of flat PV panels, such as mismatch, connections, shading, soiling, amongst others.

Due to lack of literature reviews on this matter for this specific collector technology the electrical system losses implemented in this study were set at 11%, for the reasons mentioned previously. The thermal losses were accounted for 10% (ESTIF, 2007). It is expected that due to the specific reflector geometry the impact of these parameters to be higher than the ones presented previously, leading to a deviation from the real measurement and simulated data.

For the given system, an electrical yield of 42 kWh/m^2/year was measured, being 11%$_{rel}$ lower than the simulated data (corresponding to a performance ratio of 0.89). The variation of the simulated and measured specific electrical yield for the system is given by Fig. 8.

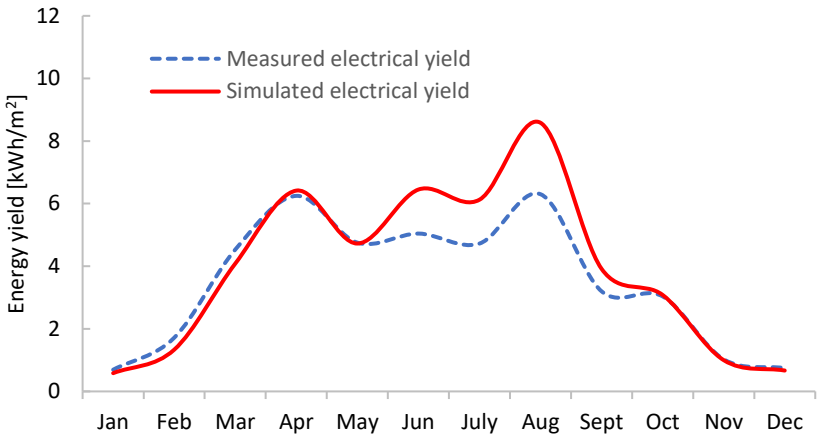

Fig. 8. Comparison between the simulated and measured electrical data for the given system.

As can be seen in Fig. 8, the relevant difference between the simulated and measured electrical data goes from May until October. This discrepancy can be explained due to the fact that the sun in summer times has a higher solar latitude, thus creating shadowing in the prototypes mounted below, as well as at some times of the day the sun passes over the 0° in the transversal direction, lowering the electrical output of the bottom receiver. As mentioned previously, the prototypes have two strings layout per receiver side and that makes them even more sensitive to shadowing than if a higher string cell layout would be employed. This phenomenon can be applied as well to the PV cell size. Since the heating load during the summer is lower than the winter, the collector provides maximum thermal power during the winter season at high latitudes, due to their asymmetric design that has the ability to concentrate the low solar altitude rays into the absorber, as can be seen in Fig. 6 (from October until May).

On the other hand, a thermal yield of 72 kWh/m^2/year was measured, or 14%$_{rel}$ lower than the simulated thermal data. This leads to a performance ratio of 0.86. The variation of the simulated and measured specific thermal yield for the system is given by Fig. 9.

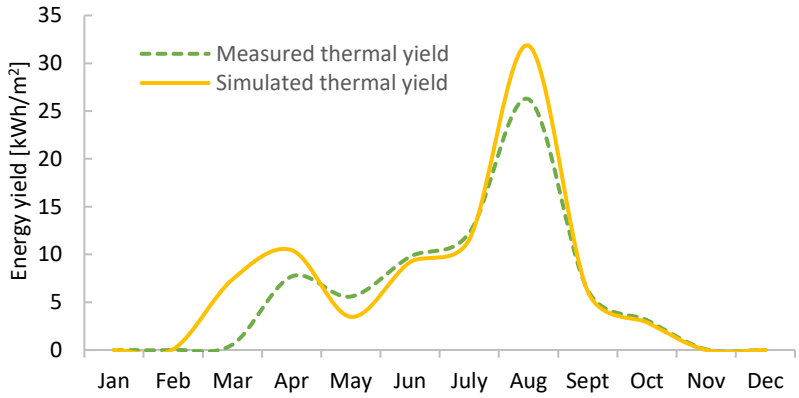

Fig. 9. Comparison between the simulated and measured thermal data for the given system.

The shadowing effect on the thermal system has less impact than in the electrical system, nevertheless, it leads to a lower energy yield. Note that the given simulated mean temperature is constant throughout the year, which can lead to differences as the ones observed in Fig. 9. The measured thermal yield of the system takes into account the variations of the temperature inside the prototype concept, which again can lead to lower energy yields.

4. Discussion

The study showed that this collector technology is very sensitive to the different inlet and outlet temperatures, which leads to a thermal performance system of 72 kWh/m^2/year or 14% lower than the simulated data. The higher inlet temperatures lead to a higher PV cell temperature, thus lowering the electrical yield of the system to 42 kWh/m^2/year or 89% of the simulated electrical yield. However, on the electrical side, the manual

production of the cell strings has an influence that is visible in the differences between the outputs of the individual collectors. The shading created by the prototypes placed above, was not taken into account in the simulations and it is estimated to cause an underperformance higher than the 2% for soiling and 3% for shading, due to the fact that a concentrating solar collector is more sensitive to shadowing than a flat PV module.

5. References

Adsten, M., Helgesson, A., Karlsson, B., 2005. Evaluation of CPC-collector designs for stand-alone, roof- or wall installation. Sol. Energy 79, 638-647.

Bernardo, R., Davidsson, H., Gentile, N., Gomes, J., Gruffman, C., Chea, L., Mumba, C., Karlsson, B., 2013. Measurements of the Electrical Incidence Angle Modifiers of an Asymmetrical Photovoltaic/Thermal Compound Parabolic Concentrating-Collector. Engineering 5, 37-43.

Copernicus Atmosphere Monitoring Service, 2018. http://www.soda-pro.com/web-services/radiation/cams-radiation-service

Dobos, A., 2014. PVWatts Version 5 Manual. NREL/TP-6A20-62641.

Duffie, J.A., Beckman, W.A., 2013. Solar Engineering of Thermal Processes. John Wiley & Sons, New York.

Gomes, J., Diwan, L., Bernardo, R., Karlsson, B., 2014. Minimizing the Impact of Shading at Oblique Solar Angles in a Fully Enclosed Asymmetric Concentrating PVT Collector. Energy Procedia 57, 2176-2185.

European Solar Thermal Industry Federation, 2007. Objective methodology for simple calculation of the energy delivery of (small) Solar Thermal systems.

Heydenreich, W., Müller, B., Reise, C., 2008. Describing the world with three parameters: a new approach to PV module power modelling. In: Proceedings of the 23rd European Photovoltaic Solar Energy Conference and Exhibition, September 1–5, 2008, Valencia, Spain.

ISO 9806, 2013. ISO 9806:2013 Solar energy - Solar thermal collectors – Test methods.

Kramer, K., Helmers, H., 2013. The interaction of standards and innovation: Hybrid photovoltaic-thermal collectors. Sol. Energy 98 (Part C), 434-439.

Lämmle, M., Kroyer, T., Fortuin, S., Wiese, M., Hermann, M., 2016. Development and modelling of highly-efficient PVT collectors with low-emissivity coatings. Sol. Energy 130, 161–173.

Lämmle, M., Oliva, A., Hermann, M., Kramer, K., Kramer, W., 2017. PVT collector technologies in solar thermal systems: A systematic assessment of electrical and thermal yields with the novel characteristic temperature approach. Sol. Energy 155, 867-879.

Mills, D.R., Giutronich, J.E., 1978. Asymmetrical non-imaging cylindrical solar concentrators. Sol. Energy 20 (1), 45-55.

Nilsson, J., 2005. Optical Design and Characterization of Solar Concentrators for Photovoltaics. Lund University.

Rabl, A., 1976. Comparison of solar collectors. Sol. Energy 18 (2), 93-111.

Serrats, E. M., Kovacs, P., Kramer, K., Nielsen, J. E., 2012. IEA-SHC Task 43: Research and standardization on solar collector testing and towards a global certification scheme. Energy Procedia 30, 162-171.

Sharaf, O. Z., Orhan, M. F., 2015. Concentrated photovoltaic thermal (CPVT) solar collector systems: Part I – Fundamentals, design considerations and current technologies. Renew. Sustain. Energy Rev. 50, 1500-1565.

Skoplaki, E., Palyvos, J., 2009. On the temperature dependence of photovoltaic module electrical performance: A review of efficiency/power correlations. Sol. Energy 83 (5), 614–624.

Stine, W. B., Harrigan, R.W., 1986. Solar Energy Systems Design, John Wiley and Sons, New York.

Tripanagnostopoulos, Y., Yianoulis, P., Papaefthimiou, S., Zafeiratos, S., 2000. CPC solar collectors with flat bifacial absorbers. Sol. Energy 69 (3), 191-203.

Welford, W. T., Winston, R., 1989. Chapter 4 – Non-imaging concentrators: The compound parabolic concentrator in High Collection Nonimaging Optics, Eds. Academic Press, 53-76.

Werner, S., 2017. District heating and cooling in Sweden. Energy 126, 419-429.

Woyte, A., Nijs, J., Balmans, R., 2003. Partial shadowing of photovoltaic arrays with different system configurations: literature review and field test results. Solar Energy 74, 217-233.

Zondag, H.A., 2008. Flat-plate PV-Thermal collectors and systems: A review. Renew. Sustain. Energy Rev. 12 (4), 891–959.